Dispersion of a suspension plug in oscillatory pressure-driven flow

Francis R. Cui, Amanda A. Howard, Martin R. Maxey, and Anubhav Tripathi

Phys. Rev. Fluids **2**, 094303 — Published 22 September 2017

DOI: 10.1103/PhysRevFluids.2.094303

Dispersion of a suspension plug in oscillatory pressure-driven flow

Francis R. Cui,[1] Amanda A. Howard,[2] Martin R. Maxey,[2,*] and Anubhav Tripathi[1]

[1]*School of Engineering, Center for Biomedical Engineering, Brown University, Providence, RI 02912*

[2]*Division of Applied Mathematics, Brown University, Providence, RI 02912*

(Dated: July 31, 2017)

Abstract

We investigate the dispersion of finite lengths of concentrated suspended particles, or suspension plugs, in a microcapillary as they are sheared in an oscillating pressure-driven flow. In the experiments, plugs of neutrally buoyant, non-colloidal particles (90 micron mean diameter) suspended in viscous fluid at low and high concentrations are observed for various values of applied strain of this cyclic shearing flow. No significant increase in the overall plug length is seen near the centerline after numerous cycles. However, significant streamwise particle migration was observed near the walls of the capillary, becoming more pronounced with increasing strain amplitude. Related numerical simulations for a suspension plug sheared in a planar channel show similar results and elucidate the dynamics for this strongly inhomogeneous flow and the anomalous particle fluxes that develop.

PACS numbers: 47.15.G-, 47.57.E, 47.55.Kf, 47.60.Dx

Keywords: Stokes flow, Viscous suspensions, Particle dispersion

* Martin_Maxey@Brown.edu

I. INTRODUCTION

The field of microfluidics is rich with potential biomedical technologies in cell sorting and isolation, as well as applications involving transport of engineered micro- or nano-particles. The emergence of micro-scale transport of suspensions at low Reynolds number thus necessitates a deeper fundamental understanding of particle dispersion within these systems. For example, samples may consist of finite volumes of suspended particles that are flowed back and forth between stations in a microchannel. Motivated by this need, we consider the motion of a periodically sheared, finite plug of suspended, neutrally buoyant non-Brownian particles within a pressure-driven Stokes flow and the extent to which the motion is reversible. The plug is formed as a finite length of a concentrated suspension of particles, with a sharp front, bounded only by the pipe or channel walls and is free to disperse in the direction of flow as illustrated in Fig. 1. The plug is sheared in a forward flow for half a period T and then by a reversed flow. A question then is whether the plug returns to its original form or not. This question comes back to the reversibility, or not, of a Stokes suspension in shear flow. This may be posed in terms of the reversibility of individual particles or the bulk reversibility of the mean distribution of particles within the plug.

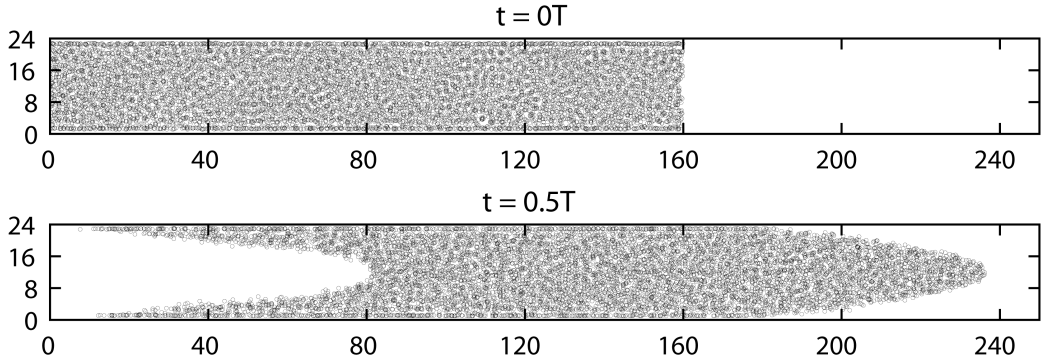

FIG. 1: Sketch of the initial suspension plug, $t = 0$, and the plug after being sheared in a Poisueille flow for a half-period, $t = 0.5T$.

Previously, Stokesian dynamics simulations for self-diffusion of particles in a steady, uniform shear flow have shown that the particle motion is generally chaotic in the long term[1]. This leaves open the question as to the source of the chaos: whether this is result of the irreversible contact forces between non-Brownian particles or the inherently nonlinear hydrodynamic interactions of multiple particles. Experiments and simulations by Pine *et al.* [2]

for oscillating uniform shear flow demonstrate that the overall self-diffusion between oscillation cycles is negligible if the strain amplitude is below a threshold level, which is lower at larger volume fraction. Subsequent studies[3–6] show that this transition between reversible and irreversible dynamics can be explained largely in terms of the contact interactions. The hydrodynamic interactions, long range or short, alone do not significantly contribute to the chaotic dynamics in contrast to the context of sedimenting particles[7]. Experiments show that the irreversible interactions and displacements between multiple particles in a Couette flow correlate with the particle roughness[8, 9].

Consideration of how a suspension plug will develop in an oscillatory flow introduces issues regarding both the degree of reversibility in a transient flow and the effects of sharp interfaces between the suspension plug and the surrounding fluid. This configuration may be compared to the dispersion of an unbounded suspension cloud in a uniform oscillating shear flow studied by Metzger and Butler [10]. The cloud is found to extend with low strain amplitude and moderate volume fraction. At high volume fractions the cloud can form a distinct shape with galaxy-like arms. For the oscillating plug we find the sharp boundaries lead to anomalous cross-stream particle fluxes.

Existing theoretical models for particle fluxes within a suspension are based on the premise of small variations in the local particle concentration or in the shear-rate, and rely on local volume-averaging and conditions of local equilibrium. The earliest of these assume a diffusive process [11, 12]. More recent suspension balance models for particle fluxes in a sheared suspension are based on an averaged momentum or force balance, whereby the particle flux relative to the suspension flow is related to the divergence of the averaged particle stress tensor and the effective hydrodynamic drag between the particle phase and the suspension as a whole[13–17]. These models give better results in representing for example the migration of particles, from regions of high shear stress towards the low shear stress near the centerline of a Poiseuille flow[13] as seen in experiments[18, 19] and numerical simulations[20]. However, they do not take into account particle layering in the near wall region and predict close packing at the center of the channel, which is not seen in experiments for low or moderate volume fractions[21]. A feature of non-Brownian suspensions is the role of particle roughness and the short-range surface repulsion that prevents direct contact of the particles as they move relative to each other in a shear flow[22, 23]. Surface roughness introduces an inherent irreversibility for the relative motion of two particles and

has been shown to modify the pair distribution function [24, 25]. This has a direct effect on the rheology and generates a resultant displacement between particles contributing to the dispersion[26, 27].

The present study is for a suspension plug, which has an initial particle volume fraction of 30% and which is oscillated forward for half a cycle and then back in a Poiseuille flow for different strain amplitudes. We examine the extent to which the motion is reversible in the bulk and how particles are redistributed. Earlier studies by Butler *et al.* [28] and by Morris [29] of a fully seeded suspension in an oscillatory Poiseuille flow suggest that at low strain amplitudes there may be an anomalous net flux of particles towards the wall, while the more usual migration to the center is seen at larger amplitudes. More recent experiments show only a migration towards the center with increasing strain amplitude and that the onset of irreversibility, in terms of self-diffusion between oscillation cycles, occurs simultaneously across the channel even though the shear rate varies across the channel[30].

The objective of the present work is to examine the change in shape of the plug over multiple oscillations and to characterize the flux of particles in the presence of a sharp variation in the concentration across the plug boundaries. Significant particle stresses and pressure may develop within the plug leading to a sharp transition in pressure at the plug front. Particle stresses may be transmitted from the near-wall region to the core leading to non-local effects on the dynamics at the plug front. Overall, this configuration of a suspension plug oscillating in a Poiseuille flow provides a clearly defined context in which to study the transient dynamics of shear-driven particle migration in the presence of concentration interfaces. Experimental results will be described in Section II, and compared to two sets of simulation results in sections III A and III B. The pre-sheared simulations in section III A correspond to the experimental conditions, while the simulations with a plug with a flat front in section III B provide greater insight into the macro- and micro-scopic irreversibility of the plug.

II. EXPERIMENTAL RESULTS

Spherical monodisperse polymethylmethacrylate (PMMA) particles of mean diameter $d = 90\,\mu\text{m}$ and density $\rho = 1.18\,\text{g}\,\text{cm}^{-3}$ were suspended in a solution comprising of equal amounts by volume of poly(ethylene glycol-ran-propylene glycol) monobutyl ether (Sigma

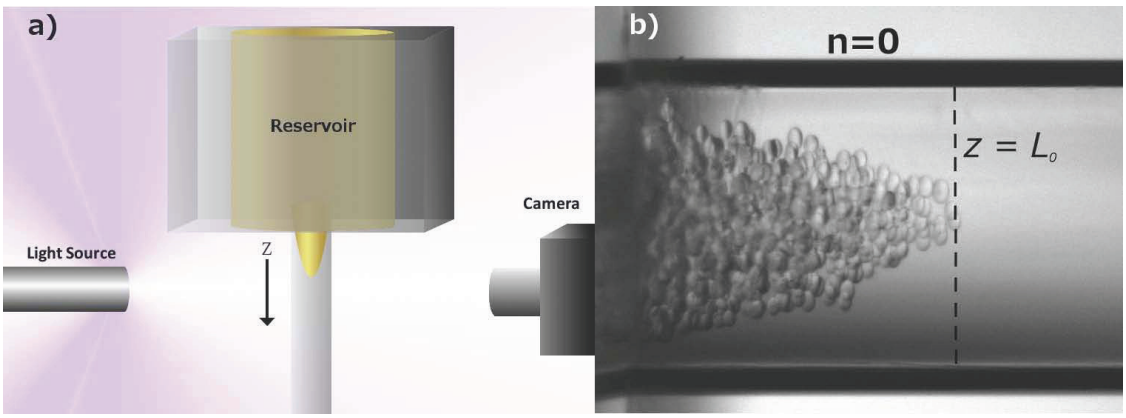

FIG. 2: (a) Schematic diagram of experimental setup. A glass capillary, connected to a syringe pump, is inserted into the suspension reservoir from below. (b) Suspension of concentration $\phi = 30\%$ is drawn in a distance $z = L_0$ and then repeatedly sheared.

Aldrich) and water, in which potassium iodide (Sigma Aldrich) was dissolved so as to match the density of the particles. The density difference $\Delta\rho$ was controlled so that a settling velocity of $d^2 g\Delta\rho/18\eta \approx 0.1\,\mu\mathrm{m\,s^{-1}}$ was achieved, thus ensuring a maximum settling distance of less than one particle diameter over the course of an experiment. The refractive index of the fluid was intentionally mismatched with that of the particles so that they were plainly visible in diffuse white light. The fluid was analyzed with a rheometer (TA Instruments) and found to be Newtonian, with a viscosity $\eta = 0.128\,\mathrm{Pa\,s}$ at 23°C. Suspensions of volume fractions 1% and 30% were prepared.

Fig. 2(a) shows the experimental design that was used to observe plug dispersion in periodic flows. Approximately 400 µL of suspension was housed in a small PDMS block with an 8 mm diameter cavity open to the atmosphere. A small entry point was punched in the bottom of the block, allowing a 2 mm glass capillary with inner diameter $D = 1.16\,\mathrm{mm}$ to penetrate the suspension. This setup ensured minimal interference from any air bubbles entrained during the mixing process, allowing them to rise to the surface and not into the plug. The capillary was connected to a 25 µL glass syringe (Hamilton) and fixed vertically so that the end submerged in the reservoir pointed upward. Both capillary and syringe were filled with the same fluid as in the suspension. Flow within the capillary was oscillated by a syringe pump (Harvard Apparatus) at various square-wave flow rates so as to not exceed a Reynolds number of $Re = 0.01$.

For each value of strain, the suspension was drawn in an initial distance of $L_0 \approx D$

from the opening of the capillary (Fig. 2(b)) and then pumped periodically for 20 cycles. For the entire range of strain amplitudes tested, the period of oscillation T remained at 10 seconds, giving flow rates that ranged from 6.0 to 39.5 $\mu L\,min^{-1}$. Images were captured at the beginning of each cycle by a CCD camera (Basler), which was fitted with a high-magnification lens and mounted on a three-dimensional traversing system. The accuracy of particle location measurements depended on the quality of the image and the degree of particle overlap. House-written MATLAB scripts were then implemented for particle tracking and counting.

For both low and high concentrations the effect of strain amplitude γ_0 on the reversibility of the plug configuration was examined by measuring the dimensionless extension $E = (z - L_0)/D$ of the initial parabolic plug front, where z denotes distance from the capillary opening. An oscillation cycle consisted of a forward motion for half a period $T/2$ followed by a reversed flow for another half period and z is measured at the end of a cycle. The strain amplitude is measured as $\gamma_0 = U_B T/D$, where U_B is the bulk velocity of the flow. This is consistent with previous studies [28, 29] and γ_0 corresponds to the ratio of the forward excursion of the plug in a half-cycle to the tube radius $R = 0.5D$. Considering previous observations[2, 10, 30] on concentration thresholds for irreversibility, we anticipated minimal dispersion for dilute concentrations, regardless of applied strain. Plug extension over time for $\phi = 1\%$ at various strain amplitudes, plotted in Fig. 3(a), indeed indicates no significant axial particle migration, with a maximum extension of 0.07 (slightly less than one particle diameter) for all γ_0. The system retains its reversibility in the bulk in spite of large amounts of accumulated strain. At this low concentration there is a dearth of hydrodynamic interactions or contacts between particles. Moreover, there seems to be a lack of correlation between extension and amount strained; final plug front positions (measured by tracking the centerline particle furthest from the capillary opening) for $\gamma_0 = 1.4$ and 5.4 remain quite close to L_0 while those for $\gamma_0 = 0.8$, 2.8 and 4.0 stray slightly further away. Any small deviations thus appear to be arbitrary and not significant. Fig. 3(a) gives then an estimate for the error in the experimental data as $\pm 0.07D$, as the plug with $\phi = 1\%$ should have zero net expansion.

With $\phi = 30\%$, we would anticipate that the particle motion is irreversible for strain amplitudes in for a significant portion of the range $\gamma_0 = 0.8 - 5.4$ considered here. If the suspension flow retains an approximately Poiseuille form, the shear rate at the tube wall is

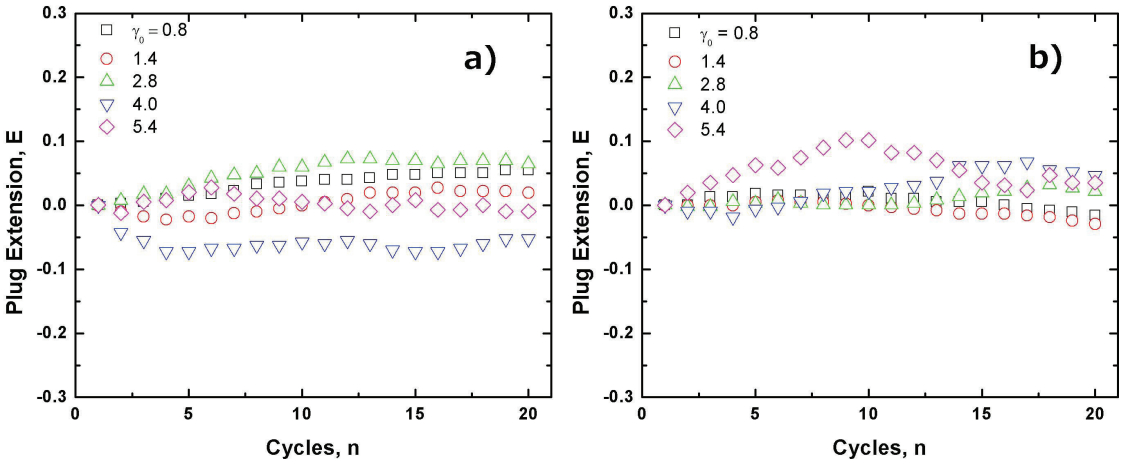

FIG. 3: (a) Plug extension E along the capillary axis for $\phi = 1\%$. The plug tip remains close to its original position L_0 throughout the duration of shearing tested. (b) Extension values for $\phi = 30\%$ are similar in magnitude to those of dilute concentrations. Strain amplitudes: $\square, \gamma_0 = 0.8$; $\bigcirc, \gamma_0 = 1.4$; $\triangle, \gamma_0 = 2.8$; $\triangledown, \gamma_0 = 4.0$; $\Diamond, \gamma_0 = 5.4$.

$4U_B/R$ and the local strain amplitude will vary linearly between zero at the centerline and $2\gamma_0$ at $r = R$. Based purely on local strain amplitudes the results for oscillating Couette flow in a fully-seeded suspension[2], the threshold for chaotic self-diffusion is a peak to peak strain amplitude of about 2. Corresponding experiments for oscillatory Poiseuille flow in a channel[30] show that the onset of irreversibility occurs simultaneously across the channel even though the local strain may be zero at the centerline. We may further compare with the experiments for particle clouds suspended in an oscillatory shear flow[10]. The sharp transition in particle concentration across the leading edge of the plug would suggest that the plug expands until the concentration drops below a threshold level for a given strain amplitude.

Results for the plug extension E, near the centerline, for $\phi = 30\%$ are shown in Fig. 3(b). We find that the plug extension measurements are close in magnitude to those of dilute suspensions and that particles along the central axial streamline remained in high local concentration, exhibiting inappreciable net particle migration. The higher concentrated suspension does however reveal a distinguishable trend in the root mean square extension with increasing γ_0; the average distance between the plug front and L_0 over 20 cycles increases with higher strain amplitudes. These values though remain relatively small for all γ_0, with E_{rms} never exceeding 0.06 (roughly $0.75d$). Although the forward-most particles

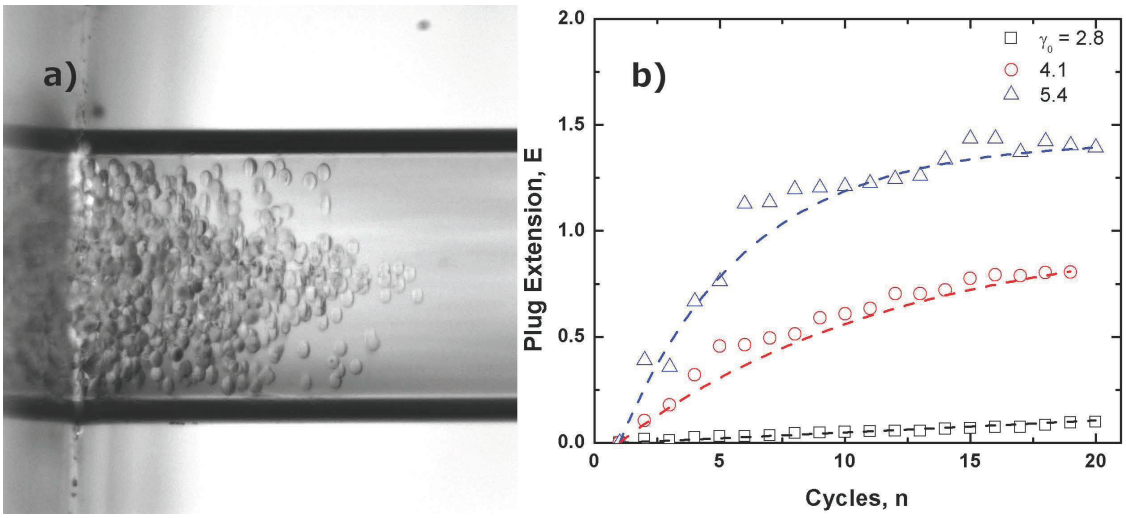

FIG. 4: (a) For $\phi = 30\%$ and $\gamma_0 = 5.4$, significant particle migration is observed near the walls while the nose of the plug displaces little. (b) Wall extension values for various γ_0 at $\phi = 30\%$ were collected by tracking the furthest particle in the near-wall regions. Strain amplitudes: $\square, \gamma_0 = 2.8$; $\bigcirc, \gamma_0 = 4.1$; $\triangle, \gamma_0 = 5.4$.

creep further away from L_0 with greater applied strain, the direction of migration along the center streamline still remains unpredictable, as the plug front seems just as likely to contract or extend. The small displacement of the plug front and its apparent impartiality towards direction of migration, even in high concentration and under high strain, suggest that the effects of particle interactions near the axis of the plug are insufficient to induce observable particle migration in the direction of flow.

Although the macroscopic bulk reversibility appears to be preserved along and near the central axis, significant particle migration near the capillary walls occurs for $\phi = 30\%$ under higher strain. At $\gamma_0 = 3.6$ to 5.4, beads at the outer radii were observed to migrate in the positive z-direction (i.e., away from the reservoir) after each successive cycle of shearing, filling the space between the parabolic plug front and walls. After 20 cycles at the highest strain, these outer beads had migrated nearly as far as $z = L_0$. Stroboscopic images reveal the chaotic nature of particle migration in the near-wall region, as beads can be displaced by several particle diameters in the streamwise direction between each period of shearing. In contrast, beads in the axial tip are never displaced by more than half a particle radius per cycle. Measurements of plug extension along the walls (shown in Fig. 4) convey the strong dispersive effect of utilizing high flow strain. While negligible near-wall particle migration

was observed for $\gamma_0 = 2.8$ and below, particle fluxes of increasing strength were observed for periodic flows of increasing strain amplitude. Outer-plug extension develops rapidly in an initial transient phase and becomes steady with accumulated strain, with the initial rate of extension increasing with strain amplitude.

III. SIMULATION RESULTS

Further insight into the dynamics of the plug development is provided by numerical simulations. Here we employ the simulation methods of Yeo and Maxey [20] to follow the evolution of a suspension plug in a pressure-driven Poiseuille flow for a channel formed between two parallel planar walls. The simulations use the force coupling method [31] to represent the particles and a Fourier pseudo-spectral scheme to compute the resulting Stokes flow. Each particle gives rise to a regularized, low-order force multipole expansion that captures the multibody hydrodynamic interactions of the particles. Additional forces and torques are included to reproduce the effects of short-range viscous lubrication interactions of particles that are not otherwise represented. The distance between the two walls, H is $12d$ or $24a$, where a is the particle radius. Periodic boundary conditions are applied in the two other directions, with $L_x = 30a$ in the spanwise direction. In the direction of the flow the channel length is chosen to be long enough so that the periodic images of the plug at maximum extension do not overlap, which gives $L_z = 320a$ in all cases except the pre-sheared case with strain amplitude $\gamma_0 = 6.39$ where $L_z = 340a$. An initial plug of 8,250 particles is introduced with uniform random seeding over a length $L_P = 160a$ as illustrated in Fig. 1 to give a particle volume fraction of 30%. The incompressible flow is computed using a resolution of 96×1024 in the x, z periodic directions, and 12 eighth-order spectral elements in the y-direction.

A short-range repulsion force between particles is introduced to reproduce the effects of surface roughness and to prevent particle overlap. As in the earlier study[20], the potential force acts along the line of particle centers $\mathbf{Y}^\alpha$ and $\mathbf{Y}^\beta$ such that the force $\mathbf{F}_P^{\alpha\beta}$ on particle α from particle β is given as

$$\mathbf{F}_P^{\alpha\beta} = \begin{cases} -6\pi a^2 \sigma_0 F_{ref} \left(\frac{R_{ref}^2 - |\mathbf{r}|^2}{R_{ref}^2 - 4a^2} \right)^6 \frac{\mathbf{r}}{|\mathbf{r}|} & \text{if } |\mathbf{r}| < R_{ref} \\ 0 & \text{otherwise,} \end{cases} \tag{1}$$

in which $\mathbf{r} = \mathbf{Y}^{\beta} - \mathbf{Y}^{\alpha}$, R_{ref} is the cut-off distance, and F_{ref} is a constant. The force parameters are chosen to limit the force to near-contact interactions with $R_{ref} = 2.01a$ and F_{ref} is set so that minimum gap between particles is about $0.005a$. A similar force is applied for near-contact of a particle and a wall. The numerical simulations assigned unit values to a and η, with an applied pressure gradient $-dp/dz = 0.08$ and time step $\delta t = 0.005$. The value of $\sigma_0 = -h\, dp/dz$ provides a reference scale for the fluid and particle stresses where $2h = H$.

The strain amplitude is based on the particle-averaged displacement $\langle \Delta Z \rangle_P$ during the forward half cycle with $\gamma_0 = \langle \Delta Z \rangle_P / h$. A constant pressure gradient is applied for each half cycle, but is varied smoothly to give a continuous transition over $\Delta t = 2$ for the flow reversals. Typical values of the oscillation period are $T = 30, 50$ and 70, which correspond to strain amplitudes of $\gamma_0 = 2.84, 4.64$, and 6.39, respectively.

In this section, we first provide a comparison with the experiments and then use the simulations to explore more fully the dynamics within the suspension plug. We examine the particle migration and then consider the relation to the contact forces between particles and the particle pressure that they induce.

A. Plugs with pre-shear

In the first set of simulations, the plug is given an initial shear deformation to correspond to the typical initial shape seen in the experiments. The pre-shear gives a starting strain of 4.6 and the leading front of the plug advances $75a$ from $z = 160a$ to $z = 235a$. Fig. 5 shows the average streamwise displacement of the particles during a forward half cycle taken from this initial pre-sheared state at $t = 0$. While the fluid satisfies a no-slip condition at the walls, the particles adjacent to the wall can advance in a quasi-rolling motion. The profiles are not exactly parabolic but the ratio of the peak displacement to the particle-averaged value is in the range $0.64 - 0.65$.

Fig. 6 shows the development of this plug over sixteen cycles from $t = 0$ to $t = 800$ with a period $T = 50$ and strain amplitude $\gamma_0 = 4.64$. One immediate observation is that the nose of the plug does not advance from one cycle to the next as seen in the experimental observations. However, the particles near the walls show a net forward migration over several cycles, as in the experiments, blunting the shape of the plug. In Fig. 6 we have color coded

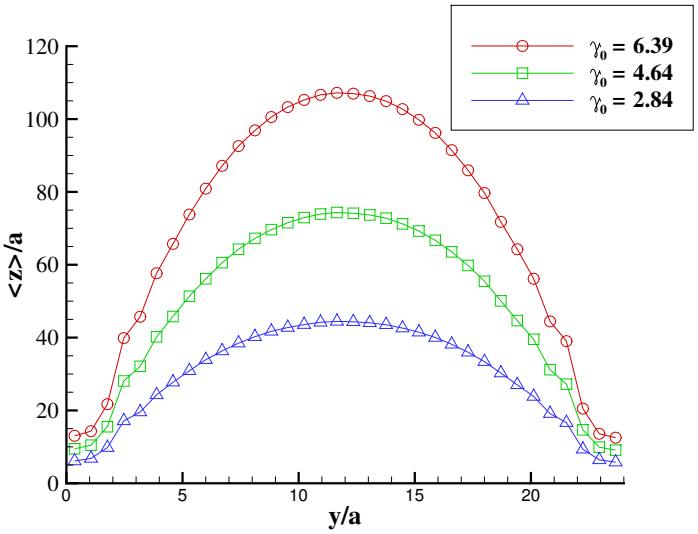

FIG. 5: Profiles of the average particle displacement $\langle Z\rangle/a$ in the streamwise direction versus y/a for a pre-sheared plug in a forward half cycle. Results are averaged over four periods for $\gamma_0 = 2.84, 4.64, 6.39$.

the particles based on their final position at $t = 16T$. The particles centered in the near wall zone $0 \leq y \leq 3a$ are shown in red, in the mid-shear zone $3a \leq y \leq 6a$ are shown in green and in the core zone $6a \leq y \leq 18a$ are shown in blue. There are corresponding red and green layers near the upper wall. The core zone spans the central width h of the channel, where the mean shear-rate would be less than half of the peak value. The other two zones are layers $h/4$ thick. We can trace from these images where the particles originate in the earlier cycles. It is seen that many of the near-wall particles at $t = 16T$ originate in the mid-shear zone within the bulk of the suspension plug earlier on and then move towards to the wall and expand towards the plug front. There is no significant migration of core particles towards the wall at the plug front even though one may expect this as a result of some shear-induced diffusion down a particle concentration gradient.

Fig. 7 provides a comparison of the near-wall forward migration E of particles at the plug front, as measured in the simulations, with the experimental results shown in Fig. 4. While we use standard definitions for the strain amplitude, essentially $\gamma_0 = \langle\Delta Z\rangle_P/R$ in the tube and $\gamma_0 = \langle\Delta Z\rangle_P/h$ in the channel, a direct comparison is difficult. The peak shear rate in a tube is $4U_B/R$ but $3U_B/h$ in a channel for a corresponding Poiseuille flow. The overall particle concentration, as shown later, does not change significantly in the present

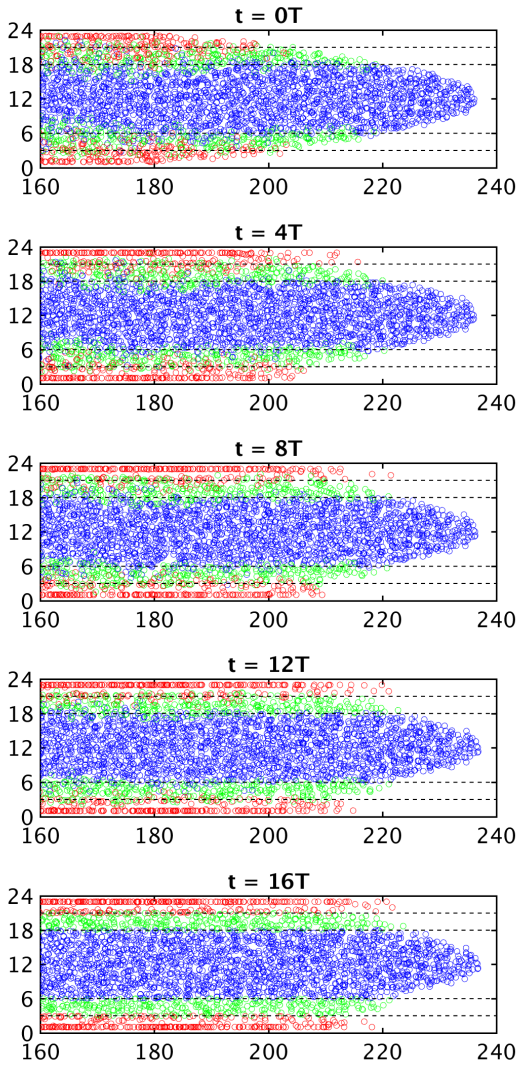

FIG. 6: Side view of particles suspended in a 3D planar channel, showing the positions at $t = 0, 4T, 8T, 12T, 16T$, for a period of $T = 50$ and strain amplitude $\gamma_0 = 4.64$. The particles are color-coded based on their position at $t = 16T$ as described in the text, the guidelines indicate the near-wall, mid-shear and core zones.

time frame and one may compare the strain rate averaged over the cross-sections in the two contexts as being representative of the particle-averaged strain rate. This gives a particle-averaged strain amplitude of $8\langle\Delta Z\rangle_P/3R$ for a tube and $1.5\langle\Delta Z\rangle_P/h$ for a channel. The results for $E = (Z - L_0)/D$ and $E = (Z - L_0)/H$, shown in Fig. 7, are in terms of the strain amplitude for a tube, while the amplitude for a channel is scaled by a factor of 4.5/8 so as to match the estimated particle-averaged strain amplitudes. The simulation results fall within the range of the experimental data and indicate that they are consistent. Exact

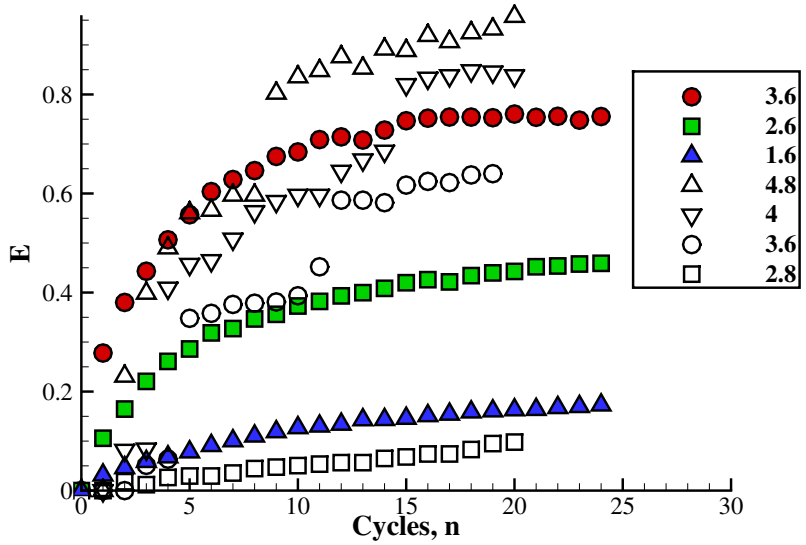

FIG. 7: Comparison of the experimental results for the near-wall extension E of the plug in a tube (open symbols) with the simulation results in a channel (filled symbols) after n oscillation cycles. The legend shows the strain amplitudes for a tube, while the values for a channel are scaled to match the estimated particle-averaged strain amplitudes.

agreement is not expected due to the differences in geometry, limitations of the rescaling, and experimental error. Experimental data was also collected for $\gamma = 5.4$, where E/D was 1.4 after twenty cycles.

B. Plugs without pre-shear

The second set of simulations are based on a suspension plug without pre-shear so the plug has an initial flat profile at both the tail $z = 0$ and at the front $z = 160a$, as in the illustration Fig. 1. This makes the effects of near-wall migration on the forward front, $z = 160a$, more obvious. The first results shown in Fig. 8 are counterparts to Fig. 6 and show the side view of the leading section of the plug for the region $z \geq 120a$ over eight oscillation periods for a low and a high strain amplitude. The same color coding of the particles is used with colors set here by the locations at $t = 8T$. We first note that the central region of the plug (blue) has a transient forward motion in the first cycle but then does not advance further. The front remains sharp here, with the local, sectionally averaged

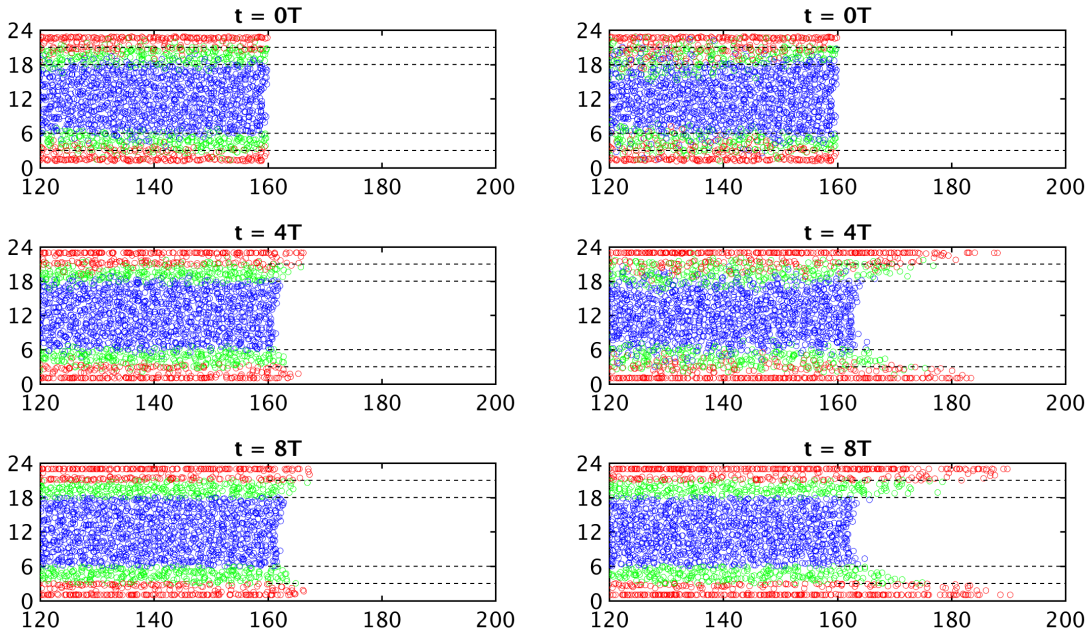

FIG. 8: Side view of particles suspended in a 3D planar channel, showing the positions at $t = 0, 4T, 8T$: (Left) period $T = 30$ and strain amplitude $\gamma_0 = 2.84$; (Right) period $T = 70$ and strain amplitude $\gamma_0 = 6.39$. The particles are color-coded based on their position at $t = 8T$ as described for Fig. 6.

volume fraction in this region still varying from 30% to 0 over a distance of one particle diameter, d.

The irreversible forward migration of the near-wall particles continues to grow in time and is stronger with the larger strain amplitude. Given the differences in the periods, the accumulated strain at $t = 8T$ for the lower amplitude case is comparable to the accumulated strain at $t = 3.6T$ for the higher amplitude case. The results for the latter at $t = 4T$ shown in Fig. 8 (right) show a much stronger response. As seen in Fig. 6, many of the near-wall (red) particles originate earlier in the mid-shear zone. There is also an appreciable forward migration of particles ending up in the mid-shear zone for this higher amplitude.

Fig. 9 shows more detail of both the plug front and tail for an intermediate strain amplitude, $\gamma_0 = 4.64$ or period $T = 50$. The small initial displacement of the otherwise stationary plug front in the core is again evident, yet it remains sharply defined. The color-coding of the particles again illustrates the forward migration of particles at the wall and that they originate within the body of the plug and migrate towards the wall, primarily from the mid-shear zone. Tracing the trajectories of particles in the mid-shear green region

that migrate to the near-wall red region shows that on average the particles migrate into the near-wall region during the forward motion on the first half period, then remain with the same y-coordinate as they migrate backward on the second half-period. Because they migrate from a region with a higher streamwise velocity, the particles do not return to their initial streamwise position, causing the extension of the plug along the channel walls.

The development of the tail of the plug is more complex. A portion of the tail region is shown in Fig. 9 for $z \leq 20.0a$ and at the two times $t = 8T$ and $t = 16T$. Here there are 1047 particles shown, based on their initial location. Over the initial interval, $t = 0 - 8T$, there is an upstream migration of particles in the mid-shear (green) zone, with minimal upstream migration in the near-wall zone. The core zone (blue) migrates downstream. Across the channel section, there is primarily a net exchange of particles from the core (blue) zone to the mid-shear (green) zone. The total number of particles in the core zone falls by 10% with increases in the number of particles in the other two zones, but mostly giving a 20% increase in the mid-shear zone. In the next interval, $t = 8T - 16T$, the trend reverses with an increase of particles in the core zone coming mostly from the mid-shear zone as particle migrate towards the centerline. The structure of the oscillation cycle implies that a particle can only substantially migrate upstream in the tail if it is initially closer to the wall in the forward half cycle than on the return half cycle. This is consistent with the net migration of near-wall particles to the mid-shear zone in the initial interval $t = 0 - 8T$.

We now consider the particles in the mid-section of the suspension plug that are removed from the direct effects of the plug front or tail. The transport in and out of these regions is quantified by a series of tables for particles originally in the mid-section, $20a \leq z \leq 140a$. As the flow is unsteady and spatially varying in two directions, plotting profiles of particle fluxes is unreliable and these tables provide a more robust overview for the exchange of particles between the different zones over the interval $t = 0$ to $t = 16T$. Table Ia covers the low strain amplitude $\gamma_0 = 2.84$ or $T = 30$ and Table Ib is for $\gamma_0 = 6.39$ or $T = 70$. The rows give the number of particles initially in each zone and the columns give the number in a zone at $t = 16T$. For the oscillating suspension plugs there is a systematic increase in the number of near-wall particles (red) and this is more pronounced at higher strain amplitude. There is a corresponding decrease in the number of particles in both the mid-shear (green) and core (blue) zones. The off-diagonal entries show the two-way exchange of particles between zones. For example, in Table Ib, there is migration of 226 particles from the wall zone to

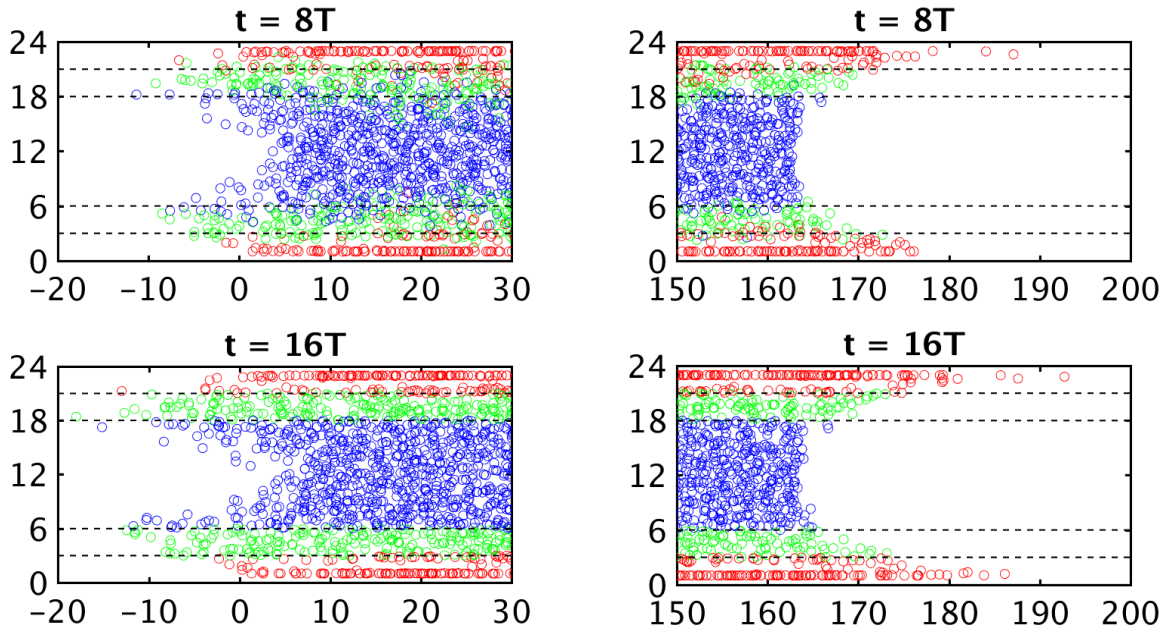

FIG. 9: Particle locations in the tail region of the plug (left) and front region (right) for oscillation period $T = 50$ ($\gamma_0 = 4.64$). Particles are color-coded by their locations at $t = 16T$ and are shown at $t = 8T$ (top row) and $t = 16T$ (lower row).

the mid-shear zone with a counterbalancing migration of 551 particles in the other direction leading to a net transfer to the wall zone. There is also a smaller net transfer of particles from the core (blue) zone to the near-wall zone. Other choices for the division of the channel into zones were evaluated and found to give similar conclusions. There was no special effect from selecting the boundary of the near-wall zone at $y/a = 3$ versus 3.25 or 3.5,

There is then a clear indication of a net transfer of particles from the mid-shear and core zones towards the walls. This is contrary to the usual expectation for developing Poiseuille flows under a constant pressure gradient where the particles migrate towards the core leaving a reduced particle concentration closer to the walls. With any Poiseuille flow, steady or oscillating, there is a brief transient flux of particles towards the wall if there is an initial random seeding of the particles in the channel. At the outset, there is no structure to the particle distribution near the wall and as a shear flow develops the particles form an organized layer adjacent to the wall, with a first peak in the particle void fraction occurring at $y/a = 1$ or 23 [20]. Examination of a fully-seeded flow with a homogeneous pressure gradient shows that 50% of the total transfer of particles to the near-wall zone occurs within $t = 0 - 50$ and this flux then diminishes quickly. For the oscillating plugs such a transient

adjustment occurs within the first one or two oscillation cycles, however the net migration to the wall continues as the streamwise extent of the wall layer expands. Additional flux tables for $T = 50$, $\gamma_0 = 4.64$, and figures demonstrating the particle fluxes are available in Appendix A.

We now consider factors linked to the redistribution of particles within the suspension plug. First, the development of the particle void fraction profile after $t = 16T$ is given in Fig. 10 for both oscillating plugs and for a developing flow under a steady pressure gradient. The latter is taken at $t = 800$, which corresponds to the same time as the $\gamma_0 = 4.64$ flow after $t = 16T$. While the average particle volume fraction is 30%, there are peaks in the particle concentration adjacent to each wall in a layering effect, already noted. The peak values are greatest for the two oscillating flows with strain amplitudes $\gamma_0 = 4.64, 6.39$ and least for the steady pressure gradient flow. Further layering of the particles is evident near the walls, at $y/a = 3$ and 21, most noticeably for the lowest amplitude oscillating flow. By $t = 800$ or a total strain of $\gamma = 150$, the flow with the steady pressure gradient has already developed a significant peak close to the centerline, while the oscillating flows have a more nearly uniform value over the core region.

Fig. 11 shows the profiles for per cycle fluctuating mean-square displacement in the

TABLE I: Number of particles in each of three zones, near-wall (red), mid-shear (green) and core zones (blue); values show numbers of particles moving from row location to column location, with corresponding totals at $t = 0$ and $t = 16T$ for T = 30 (Ia) and T = 70 (Ib). Particles are in the central section with initial stream-wise coordinate $20a \leq z \leq 140a$. Tables for T = 50 and homogeneous fully seeded flow are available in the appendix.

(a) T = 30.

	Blue	Green	Red	Total, $t = 0$
Blue	2822	419	14	3255
Green	206	981	512	1699
Red	3	123	1104	1230
Total, $t = 16T$	3031	1523	1630	6184

(b) T = 70.

	Blue	Green	Red	Total, $t = 0$
Blue	2465	584	206	3255
Green	482	666	551	1699
Red	87	226	917	1230
Total, $t = 16T$	3034	1476	1674	6184

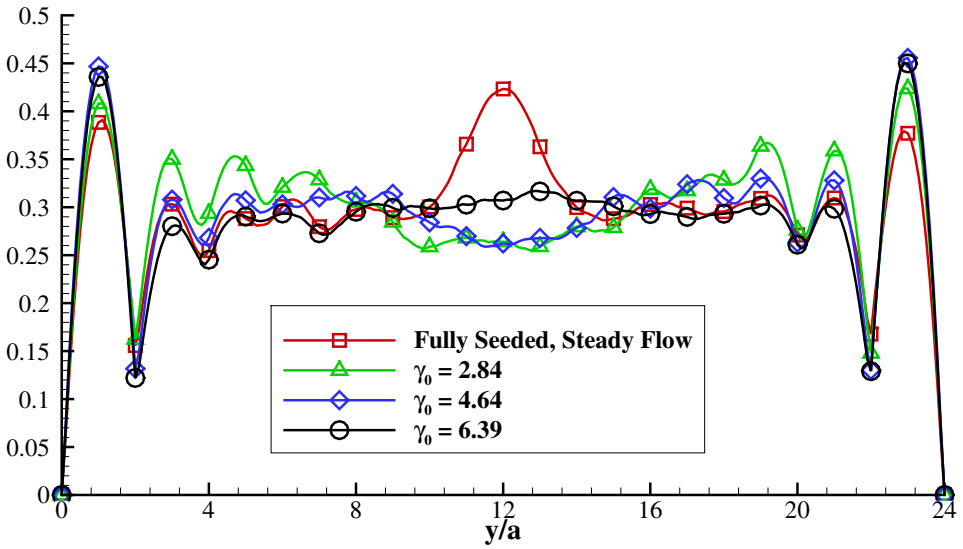

FIG. 10: Volume fraction profile for oscillating plug flows at strain amplitudes $\gamma_0 = 2.84, 4.64, 6.39$ at $t = 16T$ and a fully seeded steady flow at $t = 800$ or strain $\gamma = 150$.

streamwise and cross-stream directions averaged over the eight cycles from 8T to 16T for the three different oscillation amplitudes. These profiles reflect the self-diffusivity of the particles. In the direction of shear, the mean square displacement $\langle \Delta Y^2 \rangle / a^2$ increases with strain amplitude and is strongest at distances of $4a - 7a$ from each wall. Particles are less influenced by confining effect of the wall at these locations and fall mostly within the mid-shear (green) zone. The values for the two larger amplitudes are consistent with a scaling based on strain amplitude. The results for the mean square displacement in the streamwise direction are similar but magnified by the dispersion effect of the mean shear flow.

A key factor in the description of particle migration by suspension balance models [13, 14, 16] is the role of particle stresses and specifically the role of contact forces due to particle roughness [4–6]. Here we have computed the particle pressure due to the contact forces between particles as set by (1). The contact forces are generated as equal and opposite pairs between particles along the line of centers giving rise to a force dipole for each pair. These are summed and averaged to obtain the pressure from the trace. In an earlier study of steady Poiseuille flow [20] this pressure was found to be nearly uniform across most of the channel once the flow is fully developed.

Fig. 12 shows this particle pressure, averaged across the whole flow, in a simple Poiseuille

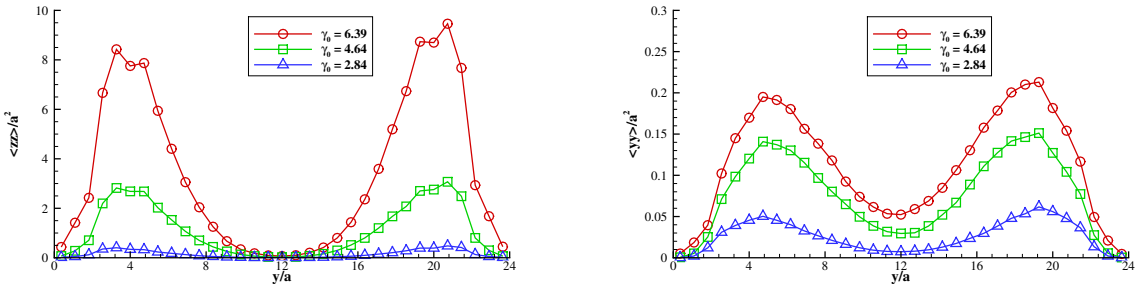

FIG. 11: Per cycle, means square displacements in the streamwise (left) and cross-stream (right) directions shown as a profile. The results are averaged over all particles in the plug, for strain amplitudes $\gamma_0 = 2.84, 4.64, 6.39$.

flow as the strain develops under a steady pressure gradient. The pressure is scaled by σ_0 and the results are shown for time $t = 0 - 200$, corresponding to strains $0 - 37$. The average particle pressure reaches the peak value by about $t = 25$ and levels off for $t > 40$ to a value consistent with previous results for this volume fraction of 30% [20]. This indicates the time scale for the initial development of particle contacts. Also shown is the particle pressure for the oscillating suspension plug with period $T = 50$ as it varies over several cycles. The pressure grows during the forward half cycle, $0 < t < 25$, drops to zero as the flow is reversed and then grows again on the reverse half cycle. The initial half cycle has a somewhat higher peak pressure as the particles rearrange from the random seeding. The peak pressure then settles to an ambient level for later cycles. When the shear flow goes to zero, any non-zero contact forces between particles will soon create the small displacements needed to reduce this force to zero.

The average profiles of the particle contact pressure, taken over the mid-section of the plug, are shown in Fig. 13 just prior to the flow reversal at several instances for the three strain amplitudes. Because of the intermittent nature of displacement and contact events observed within the front of the plug, the pressure profiles are averaged over four periods, with data taken from one time unit before the end of the period. The pressure profiles are found by:

$$\langle P \rangle(y) = \frac{1}{L_x \times L_z} \left\langle \sum_{i=1}^{N_p} \int \int P^i \chi_p^i(\mathbf{x}) \, dx \, dz \right\rangle,$$

in which P^i is the value of the particle contact pressure and χ_p^i is the indicator function of particle i.

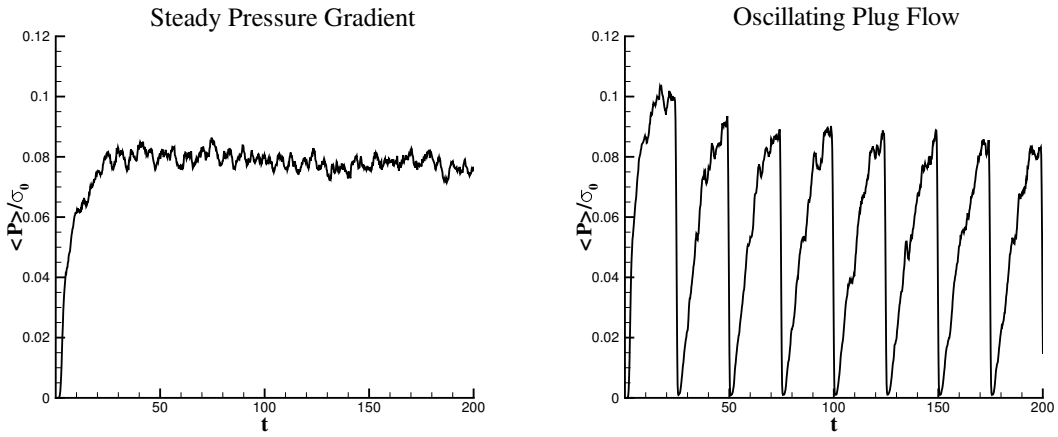

FIG. 12: (Left) Development of particle contact pressure averaged over all particles for a simple initially uniform suspension in a steady Poiseuille flow. (Right) Particle averaged contact pressure in a plug for $T = 50$ over four cycles.

Also shown in Fig. 13, as a reference, are profiles for particle contact pressure in the fully-seeded flow driven by a steady pressure gradient. This may be compared to the results for the intermediate strain amplitude. In general terms for this steadily driven flow, the particle contact pressure is greater near the wall and decreases towards the centerline reflecting the corresponding change in mean shear. The highest peaks signify the wall layer and the second layer of particles adjacent to the wall layer, which represent the red and green particles respectively. The relative heights of the two peaks are nearly balanced in the first interval shown, averaged at $t = 250, 300, 350$ and 400 labeled as $5T - 8T$, and thereafter the peak at $y/a \sim 1$ is slightly larger. By $t = 250$ the particle layer adjacent to the wall is already formed and filled, remaining little changed later on while the next layer and particles further out are more mobile. Once the wall layer is formed, the particles on average migrate towards the center of the channel.

In the first plot at $t = 5T - 8T$, the particle pressure for each oscillatory flow has a larger peak value at $y/a \sim 3$ than at $y/a \sim 1$. This is consistent with the observed migration of particles towards the wall (red zone). At $t = 13T - 16T$, the near-wall peak is higher than the mid-shear region peaks for the highest strain amplitude. This comes at a transition from the migration towards the walls to beginning a net migration to the zero shear region in the center of the channel. The peak is still greater at $y/a \sim 3$ for the two lower strain amplitude cases. These observations can be compared to the volume fraction profile in Fig.

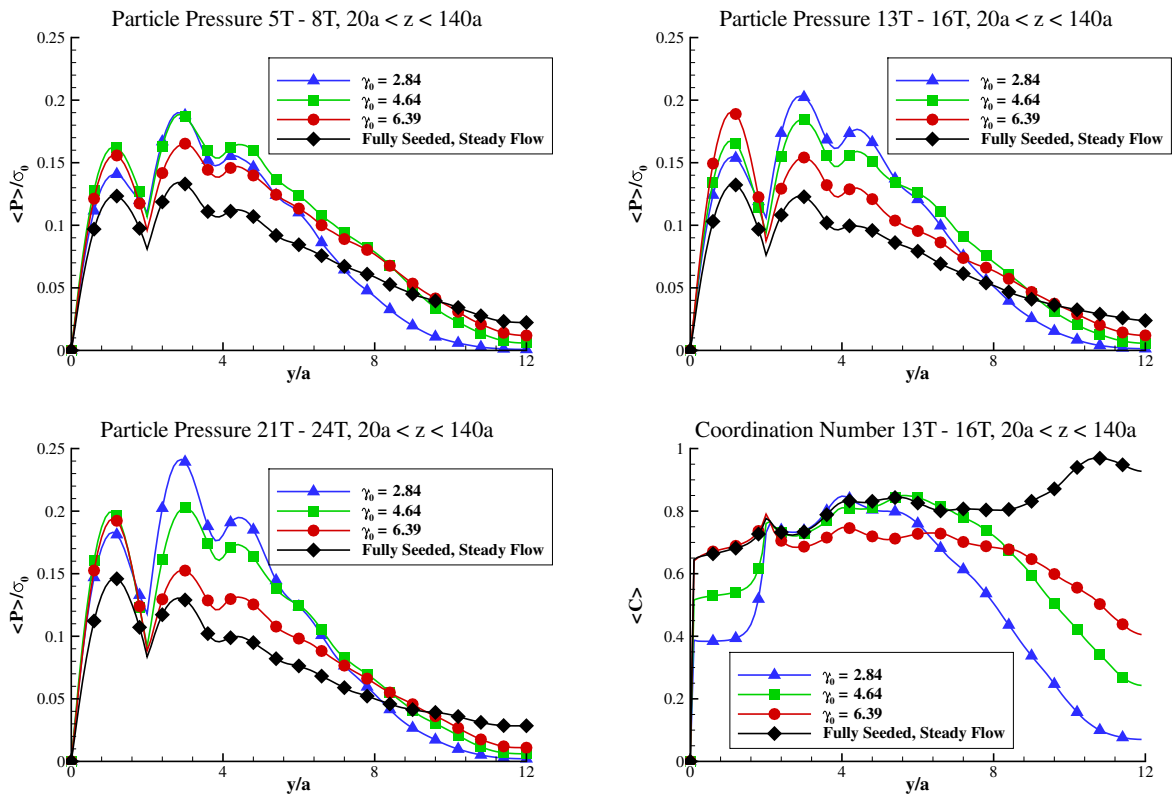

FIG. 13: Profiles of particle pressure and coordination number formed over the mid-section of the plug just before flow reversal in oscillating flow (oscillatory) or for corresponding time intervals for an initially uniform suspension with a constant pressure gradient (steady). Top left: Particle pressure at $t = 5T - 8T$ (oscillatory) and $t = 250 - 400$ (steady); top right: Particle pressure at $t = 13T - 16T$ (oscillatory) and $t = 650 - 800$ (steady); bottom left: Particle pressure at $t = 21T - 24T$ (oscillatory) and $t = 1050 - 1200$ (steady); bottom right: coordination number at $t = 13T - 16T$ (oscillatory) and $t = 650 - 800$ (steady).

10 taken at $t = 16T$. Finally, at $t = 21T - 24T$, the peaks are nearly balanced for the intermediate strain amplitude $\gamma_0 = 4.64$, while the pressure at the lowest and highest strain amplitudes are still greatest at $y/a \sim 3$ and $y/a \sim 1$, respectively. We can relate these changes to the results of Fig. 7 which show that there is no increase in near-wall extension for $\gamma_0 = 6.39$ after $t = 16T$, while $\gamma_0 = 4.64$ is only slowly increasing from $t = 16T$ to $t = 24T$. At all three intervals, the pressure at the centerline is largest for the steady case and lower for the oscillating flows. The pressure profile for the fully-seeded flow is quite similar at $t = 650 - 800$ and $t = 1050 - 1200$, and the $\langle P \rangle / \sigma_0$ drops to a value of 0.027 at

the centerline.

While we may associate a difference in contact pressure as an indicator for the net particle flux, the duration for which this pressure difference exists is equally as important in the oscillating flows. The accumulated strain at $24T$ for the lowest strain amplitude is substantially lower than for the other two. Even though the contact pressure has the greatest difference in the near-wall peaks for the lowest strain amplitude, the net migration of particles is the least. This reflects the time for the pressure to develop within a half-cycle, a more disordered state in the near-wall layers, and the time (or strain) needed for significant migration to occur within the half-cycle. Since the reversal of the flow results in an instantaneous drop in the contact pressure, the flows with higher strain amplitude, and thus more time for the contact pressure to form and act, demonstrate larger particle migrations.

Further information is provided in Fig. 13, where the profile for the coordination number is shown for the particles just prior to $t = 13T - 16T$. This measures the fraction of particles in near-contact, as determined by whether two particles are close enough to generate a contact force (1) even though the magnitude of the contact force is low. This is given by:

$$\langle C \rangle(y) = \frac{1}{\phi(y)} \frac{1}{L_x \times L_z} \left\langle \sum_{i=1}^{N_p} \int \int C^i \chi_p^i(\mathbf{x}) \, dx \, dz \right\rangle,$$

in which C^i the number of particles within a distance R_{ref} of particle i and χ_p^i is the indicator function of particle i. For the flow driven by a steady pressure gradient the coordination number is highest near the centerline where particles are migrating. For the oscillating flows it is generally greater in the mid-shear zone. In the near-wall layer, the coordination number increases with the strain amplitude, with the value for the highest strain amplitude case matching that of the constant pressure gradient. This is consistent with the wall layer reaching a fully populated equilibrium and this match of coordination number for the cases of constant pressure gradient and for $\gamma_0 = 6.39$ persists.

IV. CONCLUSIONS

In this study, we have investigated the development of a concentrated plug of suspended non-Brownian particles when subjected to oscillating, pressure-driven Stokes flow. A primary question is whether the motion of the plug, in either a circular tube or a channel, is reversible in the bulk for the plug as a whole. Both the experiments and numerical

simulations demonstrate the same features. The plug front shows minimal change or net displacement in the region near the centerline even after many oscillation cycles and over a range of strain amplitudes. In the region adjacent to the walls the particles in the plug front advance, with this being greater for larger strain amplitudes. There is an apparent minimum strain amplitude for this irreversible response in the bulk motion. The experiments and the simulations indicate that the rate of forward extension of near wall particles in the plug front becomes slower after the first $10 - 15$ cycles, and shows negligible increase after 16 cycles at the high strain amplitude $\gamma_0 = 6.39$.

This system highlights the practical issues of how samples of suspended material may be handled in microfluidic systems. A suspension plug with bulk concentration of 30% can be moved with a good degree of bulk reversibility over short distances. These results apply to the early development and dispersion of a suspension plug in unsteady flow. Due to the time scale, the long term Taylor dispersion of a suspension having gradual streamwise variations in particle concentration has not been established [32, 33].

The system also illustrates the fundamental questions posed for particle transport and particle fluxes in unsteady, inhomogeneous suspension shear flow. The interface between the suspended particles in the plug and the clear fluid outside remains sharp at the plug front in the core zone. The observed net migration of particles towards the near-wall zone for the oscillating plugs, while anomalous, appears to be consistent with the effects of particle stresses and supports the general concepts behind the suspension balance model. It is clear though that the details of how the particle stresses, and the contact forces in particular, govern the particle fluxes requires further investigation. This is especially true for the interactions between the confined near-wall zone and the more mobile mid-shear zone adjacent to it.

Several general features emerge. Noticeably for individual particles at the leading edge of the plug, movement in the cross-stream direction is observed to be associated with contact with other particles, leading to intermittent displacement events instead of a continual migration. Within the central section of the plug, away the leading and trailing edges, the particles are fully immersed in the suspension and contacts between particles can be characterized by the particle contact pressure. As the strain increases during a half-cycle the micro-structure of the sheared suspension develops and the particle pressure builds to an equilibrium level. Only if the contact pressure is sustained at this level before the flow

reverses is there significant cross-stream migration of particles.

These observations of the particle pressure indicate the important role of the particle contact forces in generating a net flux. It is clear too that this is only part of the story and further study is needed. One issue is the relative mobility of particles in the near-wall region where the finite size of the particles and the confining effects of the wall are important. Further we do not have sufficient data at this point to determine the variation of the particle stresses along the length of the plug and the extent to which the fronts at the leading and trailing ends of the plug relieve the particle stress.

ACKNOWLEDGMENTS

We would like to thank Dr. Kyongmin Yeo, now at IBM Watson Research Center for his help with the numerical simulations and Dr. Glareh Azadi for her early contributions to the experimental project. Support through an award CBET-1133106 from the National Science Foundation is gratefully acknowledged. In addition, A.A.H. acknowledges support by the National Science Foundation Graduate Research Fellowship under Grant No. DGE 1058262.

Appendix A: Extended discussion of particle fluxes

In addition to the results in Table I and Figs. 8 and 9, we provide further results for the particles in the mid-section of the suspension plug that are removed from the direct effects of the plug front or tail. Fig. 14 (left) shows the initial position of particles that fall within the mid-section, covering $20a \leq z \leq 140a$, for $\gamma_0 = 4.64$. The particles are color coded based on their positions at $t = 16T$ so that the figure shows in which region each group of particles originated. The top image shows the initial locations for particles that end up in the near-wall zone. There is a clear indication of a net transfer of particles from the mid-shear and core zones towards the walls, contrary to the usual expectation for developing Poiseuille flows. The middle image shows that there is an active exchange of particles into the mid-shear zone from both adjacent zones. The lower image indicates that some particles do migrate from the mid-shear zone to the core in the normal manner. Fig. 14 (right) shows the corresponding images for the front section of the plug, where particles are initially in

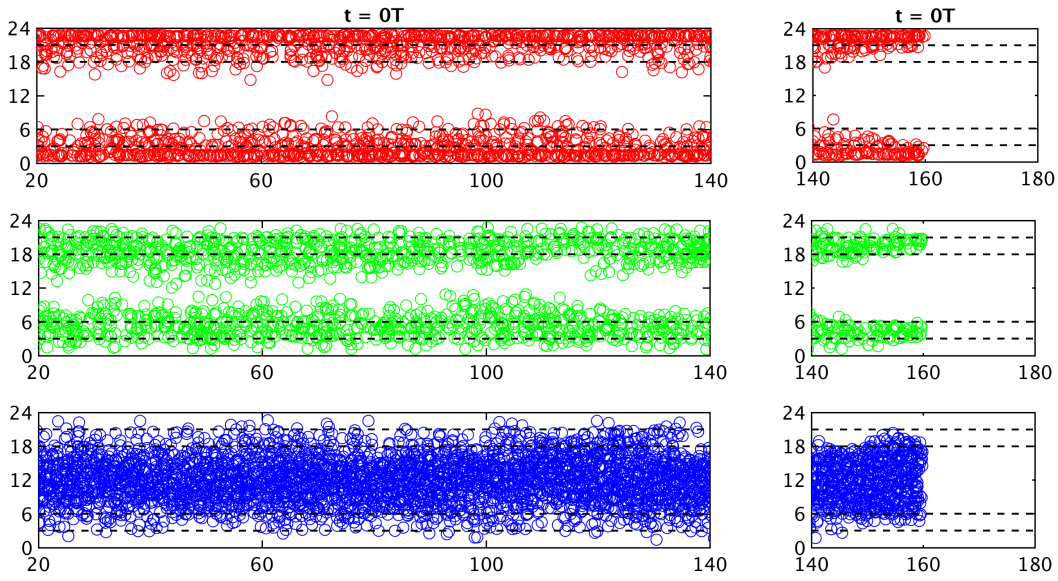

FIG. 14: (Left) Initial particle positions, at $t = 0$, based on zone locations at $t = 16T$ for $T = 50$ within the mid-section of the plug, $20 \leq z/a \leq 140$. Top image - particles in (red) near-wall zone; middle - particles in (green) mid-shear zone; bottom - particles in (blue) core zone. (Right) Similar initial particle positions for the front section of the plug, where $140 \leq z/a \leq 160$ at $t = 0$.

the interval $140a \leq z \leq 160a$. The general trends are the same as in the mid-section with particles migrating from the mid-shear zone towards the walls.

Table II gives results for $\gamma_0 = 4.64$ ($T = 50$) based on two different simulations. The two sets of data indicate the level of statistical variation in the relative numbers of particles in each zone. The results show the same trends as at the higher strain amplitude, with a systematic increase in the number of particles in the near-wall zone. As a comparison, Table IIc gives results from a simple, steadily evolving Poiseuille flow at $t = 800$. The particles in this case fully populate the channel $L_z = 160a$, are uniformly seeded at $t = 0$ and are sampled for the same mid-section. The accumulated strain is approximately $\gamma = 150$ and this example may be compared to the results in Table IIa for the intermediate strain amplitude at $t = 16T$. In this instance there is a more modest transfer of particles from the mid-shear zone to the near-wall zone, that tends to equilibrate the number of particles in each of these zones, which may be expected as they are of the same width. The number of particles in the core zone shows a small net decrease.

Similar tables were compiled for the migration of particles within the front of the sus-

pension plug to provide further information on the results shown in Fig. 14 (right). Results were compared for two different simulations with a strain amplitude $\gamma_0 = 4.64$ for particles initially in the region $140 \leq z/a \leq 160$. The total number of particles in the front for the two simulations is 1019 and 1042. After $t = 16T$, the number of particles in near-wall (red) zone for the two runs increased, with the increase coming from particles in the mid-shear (green) zone. While the initial random seeding of the near-wall zone results in fewer particles than in the mid-shear zone, this is reversed by $t = 16T$. The relative increase of particles in the near-wall zone was lower than in the mid-section in Tables IIa and IIb. There was a small increase of particles in the core (blue) zone in the front of the plug, again linked to particles migrating from the mid-shear zone.

TABLE II: Number of particles in each of three zones, near-wall (red), mid-shear (green) and core zones (blue); values show numbers of particles moving from row location to column location, with corresponding totals at $t = 0$ and $t = 16T$ for T = 50 (IIa and IIb) and a fully seeded homogeneous flow from $t = 0$ to $t = 800$ (IIc). Particles are in the central section with initial stream-wise coordinate $20a \leq z \leq 140a$.

(a) T = 50, Run 1.

	Blue	Green	Red	Total, $t = 0$
Blue	2564	565	126	3255
Green	410	737	552	1699
Red	44	180	1006	1230
Total, $t = 16T$	3018	1482	1684	6184

(b) T = 50, Run 2.

	Blue	Green	Red	Total, $t = 0$
Blue	2710	475	79	3264
Green	376	780	545	1701
Red	27	203	1019	1249
Total, $t = 16T$	3113	1458	1643	6214

(c) $t = 800$, $\gamma \approx 150$, homogeneous fully seeded flow.

	Blue	Green	Red	Total, $t = 0$
Blue	2620	492	143	3255
Green	563	698	438	1699
Red	102	247	881	1230
Total, $t = 800$	3285	1437	1462	6184

[1] German Drazer, Joel Koplik, Boris Khusid, and Andreas Acrivos, "Deterministic and stochastic behaviour of non-Brownian spheres in sheared suspensions," J. Fluid Mech. **460**, 307–335 (2002).

[2] D J Pine, J P Gollub, J F Brady, and A M Leshanksy, "Chaos and threshold for irreversibility in sheared suspensions," Nature **438**, 997–1000 (2005).

[3] Laurent Corté, P. M. Chaikin, J. P. Gollub, and D. J. Pine, "Random organization in periodically driven systems," Nature Physics **4**, 420–424 (2008).

[4] Bloen Metzger and Jason E. Butler, "Irreversibility and chaos: Role of long-range hydrodynamic interactions in sheared suspensions," Phys. Rev. E **82**, 51406 (2010).

[5] Bloen Metzger, Phong Pham, and Jason E. Butler, "Irreversibility and chaos: Role of lubrication interactions in sheared suspensions," Phys. Rev. E **87**, 052304 (2013).

[6] Phong Pham, Bloen Metzger, and Jason E. Butler, "Particle dispersion in sheared suspensions: Crucial role of solid-solid contacts," Phys. Fluids **27**, 051701 (2015).

[7] Imre Jánosi, Tamás Tél, Dietrich Wolf, and Jason Gallas, "Chaotic particle dynamics in viscous flows: The three-particle stokeslet problem," Phys. Rev. E **56**, 2858–2868 (1997).

[8] Marc S. Ingber, Andrea A. Mammoli, Peter Vorobieff, Todd McCollam, and Alan L. Graham, "Experimental and numerical analysis of irreversibilities among particles suspended in a couette device," J. Rheol. **50**, 99–114 (2006).

[9] Marina Popova, Peter Vorobieff, Marc Ingber, and Alan Graham, "Interaction of two particles in a shear flow," Phys. Rev. E **75**, 066309 (2007).

[10] Bloen Metzger and Jason E. Butler, "Clouds of particles in a periodic shear flow," Phys. Fluids **24**, 021703 (2012).

[11] David Leighton and Andreas Acrivos, "The shear-induced migration of particles in concentrated suspensions," J. Fluid Mech. **181**, 415–439 (1987).

[12] Ronald J. Phillips, Robert C. Armstrong, Robert A. Brown, Alan L. Graham, and James R. Abbott, "A constitutive equation for concentrated suspensions that accounts for shear-induced particle migration," Phys. Fluids A **4**, 30–40 (1992).

[13] Prabhu R. Nott and John F. Brady, "Pressure-driven flow of suspensions: simulation and theory," J. Fluid Mech. **275**, 157–199 (1994).

[14] Jeffrey F. Morris and Fabienne Boulay, "Curvilinear flows of noncolloidal suspensions: The role of normal stresses," J. Rheol. **43**, 1213–1237 (1999).

[15] Arun Ramachandran and David T. Leighton, "The influence of secondary flows induced by normal stress differences on the shear-induced migration of particles in concentrated suspensions," J. Fluid Mech. **603**, 207–243 (2008).

[16] Prabhu R. Nott, Elisabeth Guazzelli, and Olivier Pouliquen, "The suspension balance model revisited," Phys. Fluids **23**, 043304 (2011).

[17] M. M. Denn and J. F. Morris, "Rheology of non-Brownian suspensions," Annu. Rev. Chem. Biomol. Eng. **5**, 203–228 (2014).

[18] Christopher J. Koh, Philip Hookham, and L. Gary Leal, "An experimental investigation of concentrated suspension flows in a rectangular channel," J. Fluid Mech. **266**, 1–32 (1994).

[19] R E Hampton, A A Mammoli, A L Graham, and N Tetlow, "Migration of particles undergoing pressure-driven flow in a circular conduit," J. Rheol. **41**, 621–640 (1997).

[20] Kyongmin Yeo and Martin R Maxey, "Numerical simulations of concentrated suspensions of monodisperse particles in a Poiseuille flow," J. Fluid Mech. **682**, 491–518 (2011).

[21] Braden Snook, Jason E. Butler, and Élisabeth Guazzelli, "Dynamics of shear-induced migration of spherical particles in oscillatory pipe flow," J. Fluid Mech **786**, 128–153 (2016).

[22] P.A. Arp and S.G. Mason, "The kinetics of flowing dispersions," J. Colloid Interface Sci. **61**, 44–61 (1977).

[23] F Gadala-Maria and Andreas Acrivos, "Shear-induced structure in a concentrated suspension of solid spheres," J. Rheol. **24**, 799–814 (1980).

[24] Indresh Rampall, Jeffrey R. Smart, and David T. Leighton, "The influence of surface roughness on the particle-pair distribution function of dilute suspensions of non-colloidal spheres in simple shear flow," J. Fluid Mech. **339**, 1–24 (1997).

[25] Frédéric Blanc, François Peters, and Elisabeth Lemaire, "Experimental signature of the pair trajectories of rough spheres in the shear-induced microstructure in noncolloidal suspensions," Phys. Rev. Lett. **107**, 208302 (2011).

[26] F. R. da Cunha and E. J. Hinch, "Shear-induced dispersion in a dilute suspension of rough spheres," J. Fluid Mech. **309**, 211–223 (1996).

[27] Isidro E Zarraga and David T Leighton, "Measurement of an unexpectedly large shear-induced self-diffusivity in a dilute suspension of spheres," Phys. Fluids **14**, 2194–2201 (2002).

[28] Jason E. Butler, Paul D. Majors, and Roger T. Bonnecaze, "Observations of shear-induced particle migration for oscillatory flow of a suspension within a tube," Phys. Fluids **11**, 2865–2877 (1999).

[29] Jeffrey F. Morris, "Anomalous migration in simulated oscillatory pressure-driven flow of a concentrated suspension," Phys. Fluids **13**, 2457–2462 (2001).

[30] Jeffrey S. Guasto, Andrew S. Ross, and J. P. Gollub, "Hydrodynamic irreversibility in particle suspensions with nonuniform strain," Phys. Rev. E **81**, 061401 (2010).

[31] Kyongmin Yeo and Martin R Maxey, "Simulation of concentrated suspensions using the force-coupling method," J. Comput. Phys. **229**, 2401–2421 (2010).

[32] I M Griffiths and H A Stone, "Axial dispersion via shear-enhanced diffusion in colloidal suspensions," Europhys. Lett. **97**, 58005 (2012).

[33] Arun Ramachandran, "A macrotransport equation for the particle distribution in the flow of a concentrated, non-colloidal suspension through a circular tube," J. Fluid Mech. **734**, 219–252 (2013).